Multiple Equilibria of the Hadley Circulation in an Intermediate-Complexity Axisymmetric Model

GILLES BELLON

Centre National de Recherches Météorologiques, Météo-France, Toulouse, France

ADAM H. SOBEL

Department of Applied Physics and Applied Mathematics, and Department of Earth and Environmental Sciences, Columbia University, New York, New York

ABSTRACT

A model of intermediate complexity based on quasi-equilibrium theory—a version of the Quasi-Equilibrium Tropical Circulation Model with a prognostic atmospheric boundary layer, as well as two free-tropospheric modes in momentum, and one each in moisture and temperature—is used in a zonally symmetric aquaplanet configuration to study the sensitivity of the Hadley circulation to the sea surface temperature (SST) latitudinal distribution. For equatorially symmetric SST forcing with large SST gradients in the tropics, the model simulates the classical double Hadley cell with one equatorial intertropical convergence zone (ITCZ). For small SST gradients in the tropics, the model exhibits multiple equilibria, with one equatorially symmetric equilibrium and two asymmetric equilibria (mirror images of each other) with an off-equatorial ITCZ.

Further investigation of the feedbacks at play in the model shows that the assumed vertical structure of temperature variations is crucial to the existence and stability of the asymmetric equilibria. The free-tropospheric moisture–convection feedback must also be sufficiently strong to sustain asymmetric equilibria. Both results suggest that the specific physics of a given climate model condition determine the existence of multiple equilibria via the resulting sensitivity of the convection to free-tropospheric humidity and the vertical structure of adiabatic heating. The symmetry-breaking mechanism and resulting multiple equilibria have their origin in the local multiple equilibria that can be described by a single-column model using the weak temperature gradient approximation.

An additional experiment using an SST latitudinal distribution with a relative minimum at the equator shows that the feedbacks controlling these multiple equilibria might be relevant to the double-ITCZ problem.

1. Introduction

The intertropical convergence zone (ITCZ) is a salient feature of the earth's atmosphere: it appears on satellite images as a longitudinal cloud band near the equator. Over most of the world oceans, and in particular over the eastern Atlantic and Pacific basins, the ITCZ is located around 10°N. Why this climatological equator is not collocated with the geographical one is still poorly understood despite a considerable body of work.

Furthermore, our ability to simulate this off-equatorial rainband is limited. General circulation model (GCM) simulations have historically exhibited a second ITCZ in precipitation south of the equator in the eastern basins, where it actually does not exist [except briefly in boreal spring; e.g., Lietzke et al. (2001); Gu et al. (2005)]. This bias is so systematic that Mechoso et al. (1995) coined the term "double ITCZ syndrome." Modern GCMs, such as those used for the Intergovernmental Panel on Climate Change's (IPCC) Fourth Assessment Report (AR4), still exhibit this syndrome (Dai 2006; Bretherton 2007). Understanding the mechanisms responsible for the location (and number) of ITCZ(s) is therefore not only a theoretical challenge but also a step toward the improvement of the simulation of tropical precipitation by GCMs.

Corresponding author address: Gilles Bellon, Centre National de Recherches Météorologiques, 42, avenue Gaspard Coriolis, 31057 Toulouse, France.
E-mail: gilles.bellon@meteo.fr

The ITCZ has a propensity to be located over the warmest sea surface temperatures, but the relationship between SST and precipitation is far from perfect (Hess et al. 1993), and modeling studies have produced ITCZs and Hadley circulations even in calculations using aquaplanet boundary conditions with uniform SST (Sumi 1992; Chao and Chen 2004). In some cases the ITCZ can occur even over a SST minimum (Kirtman and Schneider 2000; Barsugli et al. 2005). It appears from the moist static energy budget that the location of the ITCZ is governed by the competition of surface fluxes (in which the SST plays an important role, but so do the surface winds) and the dynamical (mostly the moisture–convection feedbacks) and radiative contributions. Recent observations of the ITCZ in the eastern Pacific showed during the East Pacific Investigation of Climate (EPIC) campaign (2001) that the contribution of low-level convergence is about half that of local surface fluxes in the maintenance of the ITCZ north of the equator there (Raymond et al. 2006).

Early studies emphasized the role of the dynamics in the control of the location of the ITCZ. These studies proposed atmospheric mechanisms to explain the off-equatorial position of the ITCZ in the presence of an equatorial maximum of SST, based on conditional instability of the second kind (CISK). Charney (1971) postulated that the position of the ITCZ results from a balance between steady frictional convergence that increases with the Coriolis parameter and surface fluxes that decrease with decreasing SST away from the equator. Holton et al. (1971) and Lindzen (1974) showed that transient wave-CISK modes tend to develop 5°–10° away from the equator and that these modes can organize convection at the observed latitude of the ITCZ. Some observational evidence shows the propagation of convectively coupled equatorial waves in the ITCZ (Salby et al. 1991). Indeed, GCM aquaplanet simulations using the CISK-prone Kuo convective scheme (Kuo 1974) tend to systematically exhibit twin ITCZs straddling the equator, even if the maximum SST is located on the equator (Hayashi and Sumi 1986; Sumi 1992; Numaguti 1993), some with convectively coupled wave propagation along them (Hess et al. 1993). These results are nevertheless sensitive to the horizontal resolution of the GCM (Sumi 1992) and the parameterization of surface fluxes (Numaguti 1993). CISK theories have since been criticized and the associated parameterizations have been shown to overestimate the influence of the large-scale circulation and underestimate that of the local stratification (Emanuel et al. 1994).

It appears that the simulated ITCZ depends strongly on the parameterization of convection. If convection is parameterized by moist convective adjustment (Manabe

et al. 1965), aquaplanet GCMs (Lau et al. 1988; Hess et al. 1993; Frierson 2007) as well as simpler axisymmetric models (Pike 1971) tend to simulate ITCZs over the maxima of SST. Models using parameterizations based on the quasi-equilibrium theory yield a variety of results: using an axisymmetric model with Emanuel (1991)'s scheme, Waliser and Somerville (1994) obtained a weak double ITCZ straddling the equatorial SST maximum. On the other hand, use of the Arakawa–Schubert parameterization (Arakawa and Schubert 1974) in a GCM can produce an ITCZ that closely follows the SST maximum (Goswami et al. 1984; Frierson 2007). Similar work using a simplified Betts–Miller scheme produced an equatorial ITCZ over an equatorial maximum of SST (Frierson 2007).

Subsequent studies emphasized the role of atmosphere–ocean coupling. The combination of the three following coupled feedbacks could provide a symmetry-breaking mechanism under an equatorially symmetric solar forcing and cause an off-equatorial SST maximum and poleward displacement of the ITCZ (Xie and Seki 1997; Xie 2005, and references therein): (i) a feedback between the atmospheric circulation and wind-induced surface fluxes, (ii) a cloud feedback involving the subtropical stratus decks, and (iii) a feedback between the atmospheric circulation and upwelling. The selection of the hemisphere into which the ITCZ is displaced could be due to the shape of the continents on the eastern shore of oceanic basins (Xie 2005). Indeed, a better simulation of the stratus decks has been shown to improve the simulation of the east Pacific climate in coupled GCMs (Dai et al. 2003). Other studies point out to the role of the Andes in inducing subsidence in the east Pacific (Takahashi and Battisti 2007) or isolating the east Pacific from the Amazon basin (Xu et al. 2004), and thereby triggering the suppression of convection south of the equator.

Nevertheless, other modeling studies have shown that atmospheric processes alone may contain symmetry-breaking mechanisms. An early study by Pike (1971) exhibited an off-equatorial ITCZ in an axisymmetric model over a symmetric distribution of SST with an equatorial minimum. Raymond (2000) also showed that cloud radiative effects can break hemispheric symmetry. Equatorially asymmetric Hadley circulations have been obtained in aquaplanet, uniform-SST simulations using two different GCMs (Chao and Chen 2004; Barsugli et al. 2005) that happen to feature the same convective closure [the Relaxed Arakawa–Schubert (RAS) convective scheme, Moorthi and Suarez 1992]. Recent analyses of the double-ITCZ bias in GCMs have shown that coupled feedbacks tend to amplify the biases of the atmospheric models (Lin 2007; Zhang et al. 2007) as the latter

are manifest in studies of atmosphere-only models over fixed SST (e.g., Biasutti et al. 2006). This encourages further studies of the atmospheric processes that control the location of the ITCZ.

In Chao and Chen (2004), cloud radiative forcing is not necessary to break the equatorial symmetry. Surface fluxes and clear-sky radiation were found to be sufficient to obtain an off-equatorial ITCZ in the aquaplanet version of the Goddard Earth Observing System (GEOS) GCM forced by pole-to-pole uniform SST. In this study, the off-equatorial convection is attributed to the development of inertial gravity waves but the symmetry breaking is not explained. In Barsugli et al. (2005), adding to the surface fluxes and clear-sky radiation, the longwave cloud forcing appears to contribute to the maintenance of the asymmetric Hadley circulation in the atmospheric component of the National Center for Atmospheric Research (NCAR) Community Climate Model (CCM). Barsugli et al. (2005) also discovered multiple regimes depending on the value of their forcing parameter, with markedly different precipitation patterns (double ITCZ, single equatorial or off-equatorial ITCZ). Some of these regimes coexist for a finite range of this parameter, yielding multiple equilibria. The complexity of the response of these GCMs to a simple forcing calls for further study of the ITCZ dynamics in atmospheric models.

The present study uses an idealized model to further investigate the atmospheric processes that might be responsible for the symmetry breaking of the tropical circulation. Our model exhibits a behavior similar to the GCMs, with multiple equilibria, either symmetric or asymmetric about the equator, for the same boundary conditions. We study the processes that can account for the existence and stability of these equilibria. The next section describes the model, followed by our results in section 3 and a discussion in section 4.

2. Model

a. Model summary

We use a prototype to the second Quasi-Equilibrium Tropical Circulation Model (QTCM2) developed by Sobel and Neelin (2006) on the basis of the QTCM1 (Neelin and Zeng 2000; Zeng et al. 2000). The QTCM family of models is based on the Galerkin projection of the primitive equations on a limited number of reference vertical profiles derived from asymptotic solutions of quasi-equilibrium theory. In the QTCM1, the vertical structure of the wind has two degrees of freedom (one barotropic mode and one baroclinic mode) and the thermodynamical variables (temperature and humidity) each have one degree of freedom. The prototype QTCM2 used here includes an atmospheric boundary layer (ABL) that adds another degree of freedom for both dynamical and thermodynamical variables.

Our model further differs from QTCM1 by its axisymmetric equatorial β-plane configuration and its physical parameterizations: the radiation is simply represented as a Newtonian cooling, and the Betts–Miller (quasi equilibrium) convective parameterization has been modified to take into account the new thermodynamical degrees of freedom (Sobel and Neelin 2006).

The following sections provide details on aspects of the model that are of particular interest for the present study. The reader is referred to the appendix for a complete description of the model.

b. SST latitudinal distribution

We use a SST latitudinal distribution $T_s(y)$ similar to those used in the Aqua-Planet Experiment project (Neale and Hoskins 2000); it is symmetric with respect to the equator:

$$T_s = \begin{cases} T_s^{\mathrm{E}} - \Delta T_s \left[(1-k)\sin^2\left(\frac{\pi y}{2\sigma_y}\right) + k\sin^4\left(\frac{\pi y}{2\sigma_y}\right) \right], & -\sigma_y < y < \sigma_y \\ T_s^{\mathrm{E}} - \Delta T_s, & \text{otherwise,} \end{cases} \tag{1}$$

where T_s^{E} is the SST at the equator, ΔT_s is the equator − pole SST difference, and σ_y is the latitude at which the SST reaches its minimum. We use $T_s^{\mathrm{E}} = 28°\mathrm{C}$, $\Delta T_s = 30°\mathrm{C}$, and $\sigma_y = 8000$ km. Here k is a control parameter between 0 and 1 that modulates the flatness of the SST field at the equator. The climatological, longitudinally averaged observed SST corresponds to a parameter k close to 0.5. Figure 1 shows the SST latitudinal distributions for some values of k.

c. Convective available potential energy

The convection is parameterized using the Betts–Miller scheme (Betts 1986; Betts and Miller 1986) as implemented in the prototype QTCM2 (Sobel and Neelin 2006). In the Betts–Miller scheme, precipitation is proportional to a quantity similar to the convective available potential energy of the column—here denoted $\mathcal{E}$—if this quantity is positive and is zero otherwise. The reader is
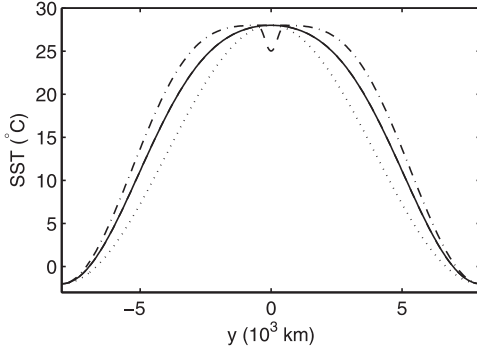
FIG. 1. SST latitudinal distributions for $k = 0$ (dotted), $k = 0.6$ (solid), and $k = 1$ (dash–dotted); SST latitudinal distribution for $k = 0.6$ with a relative minimum at the equator (dashed).

invited to read the appendix for details of the parameterization; here, we want to point out a few properties of $\mathcal{E}$ that are of interest in the next sections.

As shown in the appendix, $\mathcal{E}$ can be written as a linear combination of the thermodynamic variables:

$$\mathcal{E} = \mathcal{E}_b h_b + \mathcal{E}_q q_1 + \mathcal{E}_T T_1, \tag{2}$$

where $h_b = s_b + q_b$; $\mathcal{E}_b$, $\mathcal{E}_q > 0$, and $\mathcal{E}_T < 0$. Its time evolution can be written as follows:

$$\partial_t \mathcal{E} = \text{adv}_{\mathcal{E}} + \text{conv}_{\mathcal{E}} + \text{mix}_{\mathcal{E}} + \text{SHF}_{\mathcal{E}} + \text{rad}_{\mathcal{E}} + \text{diff}_{\mathcal{E}}, \tag{3}$$

where $\text{adv}_{\mathcal{E}}$ is the resulting effect on $\mathcal{E}$ of the advective tendencies of s_b, q_b, q_1, and T_1; $\text{conv}_{\mathcal{E}}$, $\text{rad}_{\mathcal{E}}$, and $\text{diff}_{\mathcal{E}}$ are, respectively, the contributions of convective, radiative, diffusive processes to the time evolution of $\mathcal{E}$; $\text{mix}_{\mathcal{E}}$ is the contribution of mixing at the top of the ABL, and $\text{SHF}_{\mathcal{E}}$ is the contribution of surface fluxes.

The advective contribution, $\text{adv}_{\mathcal{E}}$, can be further decomposed into the contributions of horizontal (vertical) advection by the barotropic wind $\text{adv}_{\mathcal{E}}^{0h}(\text{adv}_{\mathcal{E}}^{0v})$ and by the baroclinic wind $\text{adv}_{\mathcal{E}}^{1h}(\text{adv}_{\mathcal{E}}^{1v})$:

$$\text{adv}_{\mathcal{E}} = \text{adv}_{\mathcal{E}}^{0h} + \text{adv}_{\mathcal{E}}^{0v} + \text{adv}_{\mathcal{E}}^{1h} + \text{adv}_{\mathcal{E}}^{1v} \tag{4}$$

with

$$\text{adv}_{\mathcal{E}}^{0h} = \mathbf{v}_0 \cdot \nabla \left(\frac{\mathcal{E}_b}{\mu} h_b - \mathcal{E}_q q_1 - \mathcal{E}_T T_1 \right),$$

$$\text{adv}_{\mathcal{E}}^{0v} = (\nabla \cdot \mathbf{v}_0) \left(\frac{\mathcal{E}_b}{\mu} (h_{rb} + h_b - h^{\dagger}) - \mathcal{E}_q \frac{q_e - q^{\dagger} - M_{q0}}{\langle b_1 \rangle^F} - \mathcal{E}_T \frac{s_e - s^{\dagger} + M_{s0}}{\langle a_1 \rangle^F} \right),$$

$$\text{adv}_{\mathcal{E}}^{1h} = -\mathbf{v}_1 \cdot \nabla \left(\mathcal{E}_q \frac{\langle b_1 V_1 \rangle^F}{\langle b_1 \rangle^F} q_1 + \mathcal{E}_T \frac{\langle a_1 V_1 \rangle^F}{\langle a_1 \rangle^F} T_1 \right),$$

and

$$\text{adv}_{\mathcal{E}}^{1v} = (\nabla \cdot \mathbf{v}_1)(\mathcal{E}_q M_{q1} - \mathcal{E}_T M_{s1}),$$

where $\mathbf{V} = (0, \partial_y)$ in our axisymmetric framework.

The convection acts to reduce positive $\mathcal{E}$: it can be shown from Eqs. (A21)–(A25) that $\text{conv}_{\mathcal{E}} = -\epsilon_c \mathcal{H}(\mathcal{E})\mathcal{E}$ (where $\mathcal{H}$ is the Heaviside step function).

The contribution of the mixing at the top of the boundary layer is

$$\text{mix}_{\mathcal{E}} = \frac{p_F}{g\tau_m} [\sigma(q_{rb} + q_b - q_e) - (1 - \sigma)(s_{rb} + s_b - s_e)]. \tag{5}$$

Because $\mathcal{E}$ depends on q_b and s_b only through their sum h_b, the contribution of surface fluxes is proportional to the total surface heat flux:

$$\text{SHF}_{\mathcal{E}} = \mathcal{E}_b \frac{g}{p_B} (E + H). \tag{6}$$

The contribution of radiation is

$$\text{rad}_{\mathcal{E}} = \mathcal{E}_b \langle Q_r \rangle^b + \mathcal{E}_T \langle Q_R \rangle^F, \tag{7}$$

and the contribution of diffusion is the simple diffusion of $\mathcal{E}$:

$$\text{diff}_{\mathcal{E}} = k_q \nabla^2 \mathcal{E}, \tag{8}$$

since $\mathcal{E}$ is linear in the thermodynamic state variables.

d. Kinetics of a precipitation maximum

A maximum of precipitation corresponds to a maximum of (positive) $\mathcal{E}$ and is therefore characterized by

$$\partial_y \mathcal{E}(y_p, t) = 0; \quad \partial_y^2 \mathcal{E}(y_p, t) < 0, \tag{9}$$

where y_p is the latitude of the maximum of precipitation. The time evolution of y_p can be written
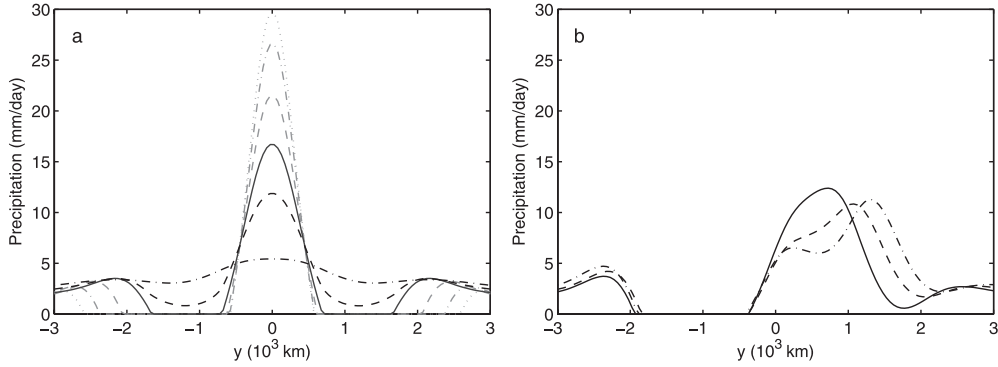
FIG. 2. Precipitation for different symmetric SST latitudinal distributions: (a) symmetric equilibrium for $k = 0$ (gray, dotted), $k = 0.2$ (gray, dash–dotted), $k = 0.4$ (gray, dashed), $k = 0.6$ (solid), $k = 0.8$ (dashed), and $k = 1$ (dash–dotted); (b) asymmetric equilibrium (with the ITCZ in the Northern Hemisphere) for $k = 0.6$ (solid), $k = 0.8$ (dashed), and $k = 1$ (dash–dotted).

$$\dot{y}_p = -\frac{\partial_t \partial_y \mathcal{E}(y_p, t)}{\partial_y^2 \mathcal{E}(y_p, t)}. \tag{10}$$

Since $\partial_y^2 \mathcal{E}(y_p, t) < 0$, $\dot{y}_p$ is of the sign of $\partial_t \partial_y \mathcal{E}(y_p, t)$.

Using Eq. (3), we can discriminate the contribution of the different processes acting on $\mathcal{E}$ to the movement of a precipitation maximum:

$$\dot{y}_p = \partial_t y_p|_{\mathrm{adv}} + \partial_t y_p|_{\mathrm{conv}} + \partial_t y_p|_{\mathrm{mix}} + \partial_t y_p|_{\mathrm{SHF}}$$
$$+ \partial_t y_p|_{\mathrm{rad}} + \partial_t y_p|_{\mathrm{diff}}, \tag{11}$$

where

$$\partial_t y_p|_X = -\frac{\partial_y X_{\mathcal{E}}(y_p, t)}{\partial_y^2 \mathcal{E}(y_p, t)}, \tag{12}$$

with $X = $ adv, conv, mix, SHF, rad, or diff.

Here $\partial_t y_p|_{\mathrm{adv}}$ can be decomposed in the contributions of the horizontal (vertical) advection by the barotropic wind $\partial_t y_p|_{\mathrm{adv}^{0h}} (\partial_t y_p|_{\mathrm{adv}^{0v}})$ and by the baroclinic wind $\partial_t y_p|_{\mathrm{adv}^{1h}} (\partial_t y_p|_{\mathrm{adv}^{1v}})$. At y_p, the precipitation is positive and $\mathrm{conv}_E = -\epsilon_c E$ has an extremum at y_p; this yields $\partial_t y_p|_{\mathrm{conv}} = 0$: the convective process itself does not participate to the movement of a precipitation maximum.

In equilibrium, for a maximum of precipitation at $y_p = y_p^{\mathrm{eq}}$, the contributions of the different processes compensate each other:

$$\partial_t y_p|_{\mathrm{adv}}^{\mathrm{eq}} + \partial_t y_p|_{\mathrm{mix}}^{\mathrm{eq}} + \partial_t y_p|_{\mathrm{SHF}}^{\mathrm{eq}} + \partial_t y_p|_{\mathrm{rad}}^{\mathrm{eq}} + \partial_t y_p|_{\mathrm{diff}}^{\mathrm{eq}} = 0. \tag{13}$$

If the system is perturbed from equilibrium, the perturbation of the location of the maximum of precipitation $\partial y_b = y_p - y_p^{\mathrm{eq}}$ follows the subsequent time evolution:

$$\dot{\delta} y_p = \delta\partial_t y_p|_{\mathrm{adv}} + \delta\partial_t y_p|_{\mathrm{mix}} + \delta\partial_t y_p|_{\mathrm{SHF}} + \delta\partial_t y_p|_{\mathrm{rad}}$$
$$+ \delta\partial_t y_p|_{\mathrm{diff}}, \tag{14}$$

where

$$\delta\partial_t y_p|_X = \partial_t y_p|_X - \partial_t y_p|_X^{\mathrm{eq}}, \tag{15}$$

with $X = $ adv, mix, SHF, rad, or diff.

3. Results

a. Multiple equilibria: Symmetry breaking

We perform simulations with varying k, using different initial conditions. For k between 0 and $k_c \approx 0.55$, the model has one stable equilibrium with a latitudinal distribution of precipitation symmetric about the equator where it has its maximum. For $k > k_c$, the model has three stable equilibria: one symmetric about the equator (in terms of precipitation) and the others asymmetric with respect to the equator, mirror images of one another. In the following, we will present results for the asymmetric equilibrium with the ITCZ in the Northern Hemisphere only. The other asymmetric equilibrium (with the ITCZ in the Southern Hemisphere) has identical properties. Figure 2 shows the precipitation in the symmetric equilibrium and the asymmetric equilibrium for different values of k.

In the symmetric equilibrium, there is one ITCZ on the equator; in the asymmetric equilibrium, there is one off-equatorial ITCZ. For values of k close to k_c, the ITCZ is around 1000 km north of the equator, close to the observed mean latitude of the ITCZ over the central and eastern Pacific and in the Atlantic Ocean. Either flatter SST profiles or increases in the absolute value of the SST (e.g., by adding a constant offset) lead to the

instability of the asymmetric equilibria, resulting in intraseasonal oscillations similar to those described by Bellon and Sobel (2008b). For example, a uniform SST ($T_s = 28°C$) similar to that used in GCM experiments (Barsugli et al. 2005; Chao and Chen 2004) yields one symmetric equilibrium with a very weak Hadley circulation and two asymmetric limit cycles characterized by a period in the intraseasonal range and a mean state with two off-equatorial ITCZs in the same hemisphere: one close to the equator and the other around 20°N (not shown). This precipitation is qualitatively similar to the observed (Sikka and Gadgil 1980) and simulated (Bellon and Sobel 2008b) pattern of the Asian monsoon mean state and intraseasonal variability. The existence of multiple equilibria is not sensitive to the wind-induced surface fluxes [although the intraseasonal oscillations are, as described by Bellon and Sobel (2008a,b)]. Sensitivity experiments using a constant surface wind $V_s = 6$ m s^{-1} yield similar symmetric and axisymmetric equilibria (not shown).

One possible explanation for the existence of multiple equilibria could be that the ITCZ develops either above the SST maximum at the equator (because of higher evaporation there) or above the maximum of SST Laplacian $\nabla^2 T_s$ away from the equator because of higher low-level convergence there following the Lindzen and Nigam (1987) theory (see also Sobel 2007). This explanation is not valid here. For k between 0.6 and 1, the Laplacian of SST is maximum between 29° and 33° latitude, much farther from the equator than the model off-equatorial ITCZ (see Fig. 2b). Also, when the contribution of the ABL temperature to the surface pressure (the effect described by Lindzen and Nigam) is removed following the method used in Sobel and Neelin (2006), the asymmetric equilibria still exist (not shown).

The essential result here is that, in our model, atmospheric processes alone contain symmetry-breaking mechanisms. Both the symmetry breaking and multiple equilibria are ascribable neither to cloud-radiative nor coupled ocean feedbacks, as neither is present in the model.

b. How is the position of the ITCZ determined?

1) ATMOSPHERIC PROCESSES CONTROLLING Y_P IN EQUILIBRIUM

To better understand the behavior of the model, we study the symmetric and asymmetric equilibria for $k = 0.6$. First, in equilibrium, we can study how the different terms of Eq. (13) equilibrate to determine the position of the precipitation maximum. In the symmetric equilibrium, all the terms are zero for reasons of symmetry. Figure 3a shows the different contributions in the asym-
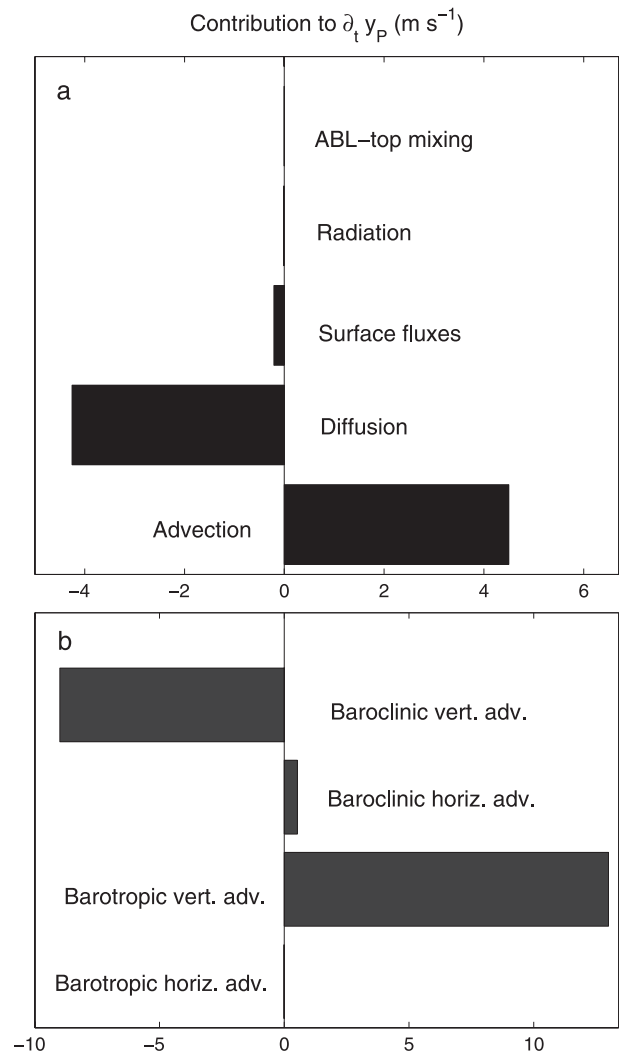

FIG. 3. Contributions of the different processes to the position of the maximum of precipitation in the asymmetric equilibrium.

metric equilibrium, and Fig. 3b decomposes the advective term into its four components.

In our model, the location of the asymmetric precipitation maximum results primarily from the balance between advection, which tends to promote convection away from the equator, and diffusion, which tends to promote it closer to the equator (Fig. 3a). The contribution of surface fluxes is much smaller than either advection or diffusion and tends to bring the precipitation maximum closer to the SST maximum at the equator. The contribution of radiation and mixing at the top of the ABL are negligible. The contribution of diffusion is proportional to the third latitudinal derivative of the precipitation (or $\mathcal{E}$). We can see from Fig. 2b that the precipitation decreases faster poleward of its maximum than it does equatorward. This results in part from the
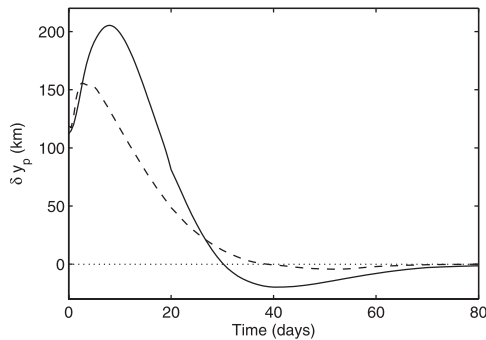
FIG. 4. Time evolution of δy_p for the symmetric equilibrium (dashed) and the asymmetric equilibrium (solid).

SST being cooler poleward of y_p than equatorward of y_p: it corresponds to a negative third derivative of $\mathcal{E}$ and therefore to an equatorward pull on the ITCZ.

The advective contribution results from the competition of the vertical advection by the barotropic mode, which pushes the ITCZ away from the equator, and by the baroclinic mode, which pulls the ITCZ closer to the equator (Fig. 3b). This corresponds to a maximum in ABL convergence north of the maximum of precipitation, and a maximum of upper-troposphere divergence south of the maximum of convection. The contribution of horizontal advection is small.

2) ATMOSPHERIC FEEDBACKS TO PERTURBATION

We perform additional experiments in which the equilibria are perturbed in the initial conditions and study the return to equilibrium. As initial conditions, we use the equilibrium fields shifted northward by 1° latitude. This experiment is used as an example to illustrate some of the feedbacks at play in the return to equilibrium, but it does not amount to a comprehensive feedback survey: other perturbations might shed light on other feedbacks.

Figure 4 shows the time evolution of the perturbation in the location of maximum precipitation $\delta y_p = y_p - y_p^{\text{eq}}$ for both the symmetric and asymmetric equilibria. In both cases, the return to equilibrium is not monotonic: the perturbation starts to grow in the first few days before it decreases and eventually changes sign before disappearing. This shows that some damped oscillatory modes are excited by the chosen perturbation. We do not describe these modes; instead, we focus on the interplay between processes during the return to equilibrium.

Figure 5a shows the contributions to the movement of the precipitation maximum, that is, the different terms in Eq. (14), in the symmetric case. The time evolution of the location of the precipitation maximum results primarily from the competition between advection (which tends to slow down the return to equilibrium) and dif-
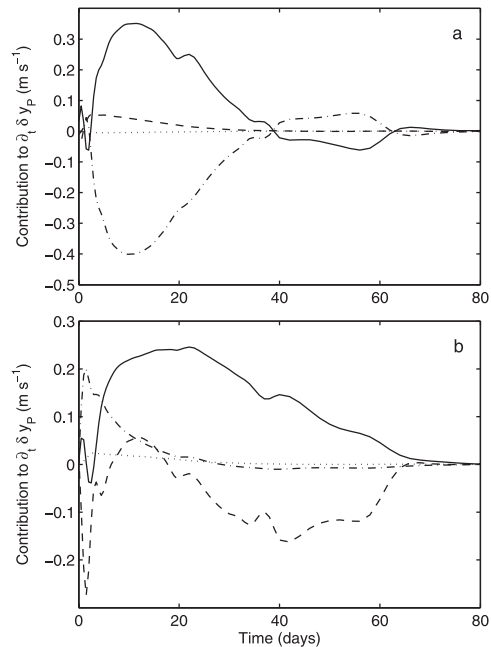

FIG. 5. Contributions of the different processes to the return to the symmetric equilibrium: (a) contributions of advection (solid), diffusion (dash–dotted), surface fluxes (dashed) and other terms (dotted) to $\dot{\delta}y_p$; (b) contributions of barotropic vertical (solid) and horizontal (dotted) advection and baroclinic vertical (dashed) and horizontal (dash–dotted) advection.

fusion (which drives the return to equilibrium). The surface fluxes constitute a third, small contribution and the other processes have a negligible impact. After the initial growth of δy_p, the advective contribution results from the combination of barotropic and baroclinic vertical advection (Fig. 5b), and the relationship between these two terms changes with time.

Figure 6a shows the contributions to the movement of the precipitation maximum in the asymmetric case. Again, the time evolution of the location of the precipitation maximum results primarily from the competition between advection (which here drives the return to equilibrium) and diffusion (which tends to increase the perturbation). Again, the surface fluxes constitute a small contribution and the other processes have a negligible impact. Compared to the symmetric case, the diffusion and advection have opposite roles, and the magnitude of the contributions is about four times larger. The advective term results from opposing contributions: the barotropic and baroclinic vertical advections. The former drives the return to equilibrium, while the latter opposes it. The horizontal advective contributions are smaller terms.

In summary, it appears that, in these experiments, the effect of the large-scale circulation competes with the effect of the horizontal diffusion of moisture. The latter
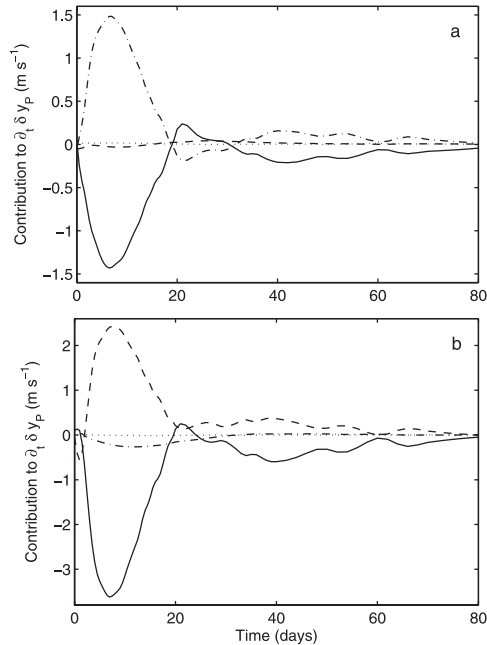
FIG. 7. Latitude of the maximum of precipitation as a function of l for the symmetric equilibrium (dashed) and the asymmetric equilibrium (solid).

FIG. 6. Contributions of the different processes to the return to the asymmetric equilibrium: (a) contributions of advection (solid), diffusion (dash–dotted), surface fluxes (dashed), and other terms (dotted) to $\dot{\delta}y_p$; (b) contributions of barotropic vertical (solid) and horizontal (dotted) advection and baroclinic vertical (dashed) and horizontal (dash–dotted) advection.

was originally introduced by Sobel and Neelin (2006) on a somewhat ad hoc basis to improve the realism of the solutions, but they suggested that it might be viewed as standing in for horizontal moisture transport by transient eddies. The observationally based analysis of Peters et al. (2008) supports this interpretation, providing some basis for further study of these solutions despite the crudeness of the diffusivity as a modeling device. The dynamical contribution results from a partial cancellation between the vertical advection by the barotropic and the baroclinic modes. This shows that the vertical structure of the wind produced by the model is crucial to the existence of multiple equilibria. It seems interesting to investigate the sensitivity of our results to the imposed wind profile V_1. This profile is linked to the perturbation temperature profile a_1 (that is also, by construction, the imposed heating profile). We can therefore study the sensitivity of our model to a_1. Doing so, the sensitivity that we investigate is not restricted to that of the profile of the wind but also includes all the effects of the sensitivity to the temperature profile.

c. Sensitivity to the temperature profile

To investigate this sensitivity we choose to modify the temperature profile by increasing and decreasing the variations of a_1 with altitude while keeping the general
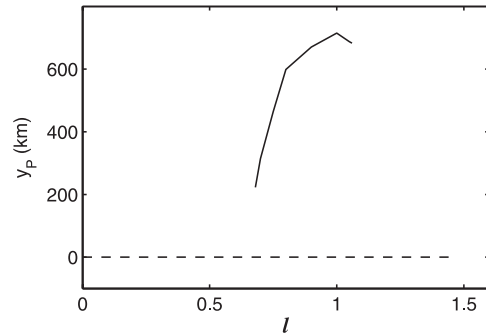
shape of the profile. We replace $a_1(p)$ by the following profile, $a_1'(p)$:

$$a_1'(p) = a_1(p_e) + l \times (a_1(p) - a_1(p_e)), \quad (16)$$

where l is systematically varied between 0 and 2, with $l = 1$ being the control value. As examples, Fig. A1 shows $a_1'(p)$ for $l = 0$ and $l = 1.5$, as well as the corresponding horizontal and vertical wind profiles.

Figure 7 shows the location of the precipitation maximum in equilibrium as a function of the parameter l (k is still set to 0.6). It appears that a stable asymmetric equilibrium exists only for a limited range of l (0.67 to 1.07). Furthermore, the location of the precipitation maximum is very sensitive to l: the latitude of the precipitation maximum is multiplied by a factor of 3 within this limited range. By comparison, the symmetric equilibrium is stable for a larger range of l (0 to 1.45).

Some elements of interpretation can be provided for the increase of the latitude of maximum precipitation with l. The larger l, the more top heavy the heating profile and the wind profile; increasing l thus yields more efficient vertical advections $\mathrm{adv}_{\mathcal{L}}^{0h}$ and $\mathrm{adv}_{\mathcal{L}}^{1h}$ for given barotropic and baroclinic divergences. This increases the influence of advection that, as a whole, tends to move the ITCZ poleward (see Fig. 3a). Because of the very intricate feedbacks at play, we do not understand well how the competition between baroclinic and barotropic vertical advections plays out to yield this response that is in line with the influence of advection in the control case.

This result is reminiscent of earlier GCM studies in which the role of the stratification was shown to be essential to the position of the ITCZ (Numaguti 1993) and in which the ITCZ dynamics were shown to be sensitive to the parameterization of convection (Numaguti 1993; Chao and Chen 2004; Frierson 2007). Different convective schemes yield different heating profiles, and changing
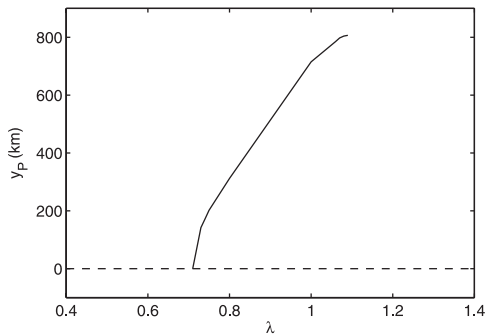
FIG. 8. Latitude of the maximum of precipitation as a function of λ for the symmetric equilibrium (dashed) and the asymmetric equilibrium (solid).

the parameterization of convection therefore changes the regime of Hadley circulation that can be simulated by the GCM in a similar way as changing the vertical structure of the temperature perturbation in our simple model. A recent experiment (Bacmeister et al. 2006) showed that increasing rain reevaporation reduces the double-ITCZ bias in the NASA GEOS GCM. We can speculate that rain reevaporation reduces the heating in the midtroposphere, therefore increasing the top-heaviness of the convective heating profile. The sensitivity of this GCM might result from the same mechanisms as in our simple model.

d. Free-tropospheric humidity–convection feedback

1) SENSITIVITY STUDY

The expression (2) of the convective available potential energy $\mathcal{E}$ shows that convection is sensitive to the ABL moist static energy and the free-tropospheric humidity and temperature. The coefficients controlling these sensitivities are a function of the averaged perturbation profiles and critical profiles [see Eq. (A26)]. In the model, the sensitivity of convection to free-tropospheric humidity is due to downdraft effects that ventilate and dry the ABL. In nature, a large part of this sensitivity is also associated to the entrainment of midtropospheric environment air into updrafts, diluting their water vapor content.

We can vary this sensitivity systematically to understand the role of the free-tropospheric humidity–convection feedback in the existence of multiple equilibria. To do so, we vary $\mathcal{E}_q$ keeping it arbitrarily proportional to its control value:

$$\mathcal{E}_q = \lambda \mathcal{E}_q^{\text{control}}, \qquad (17)$$

where λ is a free parameter. Increasing λ increases the impact of ambient free-tropospheric humidity on the
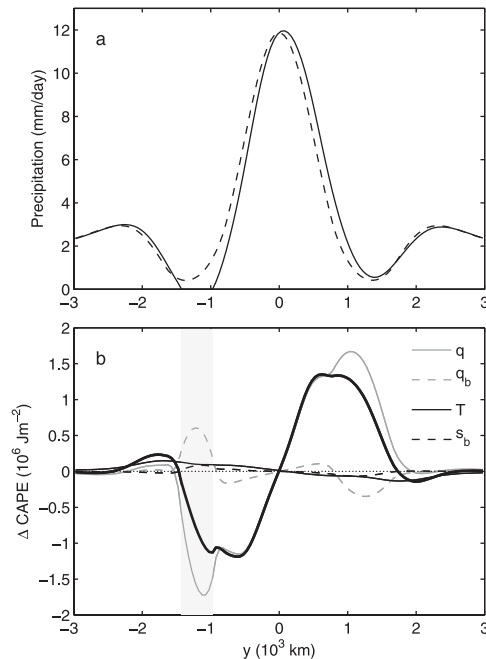

FIG. 9. (a) Precipitation in the symmetric (dashed) and asymmetric (solid) equilibria for $\lambda = 0.72$; (b) difference in $\mathcal{E}$ between the asymmetric and symmetric equilibria (thick line) and its components due to free-tropospheric humidity (gray, solid), ABL humidity (gray, dashed), free-tropospheric temperature (solid), and ABL temperature (dashed). The shaded area indicates the latitude range of suppressed convection in the asymmetric equilibrium.

convection and therefore tends to amplify the positive free-tropospheric moisture–convection feedback.

Figure 8 shows the sensitivity of the position of the ITCZ in the symmetric and asymmetric equilibria to varying λ. It appears that weakening the moisture–convection feedback (i.e., decreasing λ) reduces the asymmetry of the asymmetric equilibrium: the ITCZ gets closer to the equator. For λ smaller than a critical value $\lambda_c \approx 0.71$, the asymmetric equilibrium collapses to the symmetric equilibrium. The existence of the asymmetric equilibrium therefore requires a sufficiently strong link between convection and free-tropospheric humidity.

To better understand the bifurcation and the feedbacks that allow the asymmetric equilibrium to arise, we study the equilibria for $\lambda = 0.72$, close to the bifurcation. Figure 9a shows the precipitation for both the symmetric and the asymmetric equilibria. The two equilibria are very similar and exhibit one ITCZ surrounded by dry regions. The fundamental difference between the two is that there is a region of suppressed convection in the asymmetric equilibrium, while the symmetric-equilibrium precipitation is positive everywhere in the tropics. In the asymmetric equilibrium, the suppressed convection

in the southern tropics is associated with a northward shift of the precipitation pattern compared to the symmetric equilibrium.

Thinking of the symmetric equilibrium as a base state and of the asymmetric equilibrium as a perturbed state, we can investigate the difference between the two equilibria. Figure 9b shows the difference in convective available potential energy $\mathcal{E}$ between the asymmetric and symmetric equilibrium and the contributions of the differences in q_1, q_b, T_1, and s_b to the difference in $\mathcal{E}$. It appears that the suppression of convection in a few atmospheric columns of the southern tropics corresponds to a steady, almost antisymmetric perturbation in $\mathcal{E}$. The difference in $\mathcal{E}$ is driven by the difference in free-tropospheric humidity q_1 that is somewhat compensated by the difference in ABL humidity q_b. The differences in temperature are small, which can be explained by the tendency of the large-scale circulation to reduce gradients of free-tropospheric temperature in the tropics and by the fact that surface air temperature is closely tied to the SST. We will therefore focus on the differences in humidity between the two equilibria.

If the symmetric equilibrium is perturbed so that a nonprecipitating region appears, the free troposphere dries up and the ABL moistens in that region because convection moistens the free troposphere and dries up the ABL. While the first effect tends to maintain the suppression of precipitation, the latter effect tends to reestablish convection. The amplitude of the first, positive feedback is proportional to $\mathcal{E}_q$ and the amplitude of the second, negative feedback is proportional to $\mathcal{E}_b$. Therefore, in order to maintain the region of suppressed precipitation, convection has to be sensitive to free-tropospheric humidity, that is, λ has to be large enough, particularly compared to its sensitivity to ABL humidity.

Further study of the thermodynamic budgets shows that the main terms in these budgets are vertical advection (with both baroclinic and barotropic components) and diffusion (not shown). The ABL divergence actually decreases in the region of suppressed convection in the asymmetric equilibrium partly owing to gradients of ABL temperature, and the response of the barotropic wind therefore tends to reinitiate convection. Conversely, the baroclinic convergence increases, corresponding to a positive feedback for the suppression of convection. This suggests that the equilibria of each column in the region where convection is suppressed (or not) can be simulated in a column model as long as the large-scale vertical velocity can be parameterized. The weak temperature gradient (WTG) approximation is a method designed to parameterize the large-scale vertical velocity in a one-column framework (Sobel and Bretherton 2000). In the next section, we apply this framework to our model

and compare our WTG model to the columns of the full model in the dry subtropical regions.

2) COMPARISON TO A WTG MODEL

In the WTG approximation, the free-tropospheric temperature gradients are assumed to be very small and the horizontal advection of dry static energy is neglected. The temperature is assumed to be fixed by large-scale circulation and gravity waves and, therefore, to be constant. The large-scale vertical velocity is assumed to exactly balance the heating term in the temperature or dry static energy equation, and that assumed vertical velocity then is used to compute the large-scale vertical advection of moisture. Sobel et al. (2007) showed that a single-column model under WTG can under some conditions have two equilibria, a rainy and dry one, with the initial conditions determining which one is reached. Similar behavior can occur in a limited-area cloud-resolving model with periodic horizontal boundary conditions under WTG (Sessions et al. 2010).

In a one-column WTG model, the horizontal advection of humidity or ABL dry static energy is imposed or parameterized (Sobel et al. 2007; Sobel and Bellon 2009; Raymond and Zeng 2005). Here, as a first approximation, we neglect it. The resulting equations for the WTG model used here are given in the appendix. In the QTCM2 framework, these five equations (continuity, and budgets of energy and water in the free troposphere and the ABL) have three prognostic variables (q_1, q_b, and s_b) and three diagnostic variables ($\nabla \cdot \mathbf{v}_0$, $\nabla \cdot \mathbf{v}_1$, and $\nabla \cdot \mathbf{v}_b$). The system is thus underconstrained, and one must prescribe one of the variables to compute the equilibrium of the system. Here, we choose to prescribe the ABL divergence $\nabla \cdot \mathbf{v}_b$ (which is equivalent to prescribing $\nabla \cdot \mathbf{v}_0$ because of the continuity equation). It can be argued that at least some portion of the ABL divergence responds directly to SST gradients via the Lindzen–Nigam mechanism. This occurs exclusively in the boundary layer and thus can be considered an external forcing from the point of view of a WTG single-column model, which parameterizes the vertical velocity only in the free troposphere (Sobel 2007). Sensitivity studies show that the existence of WTG equilibria is not sensitive to this divergence as long as it is positive.

Figure 10 shows the value of the precipitation at its tropical minimum in the equilibria of the axisymmetric model as a function of λ. In the symmetric equilibrium, the subtropical precipitation minimum decreases with λ down to zero for $\lambda > 0.85$, and the asymmetric equilibrium appears with a zero-precipitation minimum $\lambda > \lambda_c$. Figure 10 also shows the precipitation in the WTG model as a function of λ, with the ABL divergence fixed to its value at the precipitation minimum in the axisymmetric
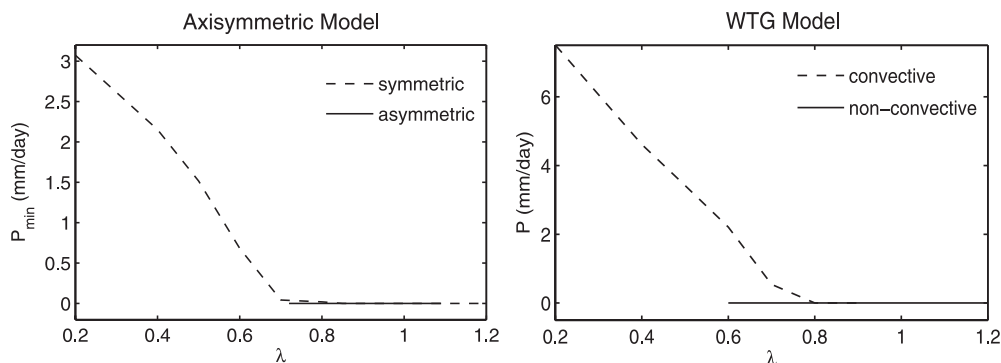
FIG. 10. (left) Subtropical precipitation minimum in the axisymmetric QTCM2 in the symmetric and asymmetric equilibria and (right) precipitation in the convective and nonconvective equilibria of the WTG model as a function of λ.

model for each value of λ. The column model captures the behavior of the axisymmetric model fairly well, exhibiting multiple equilibria with a convective equilibrium for $\lambda \lesssim 0.8$ and a nonconvective equilibrium for $\lambda \gtrsim 0.6$. The main discrepancy is that the precipitation is larger in the WTG model than in the axisymmetric QTCM2. The existence of multiple (dry and precipitating) equilibria in WTG models has been established in Sobel et al. (2007). Here, we observe that multiple equilibria of the global circulation in an axisymmetric model appear to be directly related to analogous multiple equilibria of the single column. We are not aware of other instances in which multiple equilibria of a spatially distributed dynamical system can be mapped onto multiple equilibria of a local approximation to that system at a single (albeit well-chosen) point. This result may perhaps be of some mathematical interest. In any case, it provides motivation for further study of the single-column WTG system.

e. Single and double ITCZ

Finally, we investigate the possible relevance of the multiple equilibria of the Hadley circulation on the problems of its simulation in the eastern Pacific. We perform two further simulations with a minimum of SST on the equator, a latitudinal distribution similar to the eastern Pacific SST. In practice, we use the latitudinal distribution defined by Eq. (1) with $k = 0.6$, to which an additional term, $-\delta T_s \cos[(\pi/2)y/y_{me}]$, is added for $-y_{me} < y < y_{me}$, with $\delta T_s = 3$ K and $y_{me} = 500$ km; this SST latitudinal distribution is illustrated in Fig. 1. As initial conditions, we use the symmetric and axisymmetric equilibria obtained with the original latitudinal distribution with $k = 0.6$. The two simulations reach distinct steady states. Figure 11 displays the steady-state precipitation in both cases. The symmetric initial conditions lead to a symmetric equilibrium with a double ITCZ while the asymmetric initial

conditions lead to an asymmetric equilibrium somewhat similar to the initial conditions, with one ITCZ around 10°N.

The differences between these multiple equilibria appear like a caricature of the discrepancy between the observed, asymmetric annual mean distribution of precipitation and its almost-symmetric simulation by GCMs. Our results suggest that the atmospheric component of the double-ITCZ syndrome could be interpreted as a misrepresentation of the atmospheric feedbacks that control the precipitation regimes, yielding a more symmetric regime in the GCMs compared to the real atmosphere–ocean system.

Attempts to mitigate the double-ITCZ bias have shown promises in changes of the convective parameterization (Zhang and Wang 2006) and changes in some parameters of existing parameterizations such as the lateral entrainment, reevaporation, or precipitation efficiency parameters (Terray 1998; Bacmeister et al. 2006; Li et al. 2007). These changes are a way to modify the feedbacks between humidity and parameterized convection and to modify the vertical profile of diabatic heating, hence that
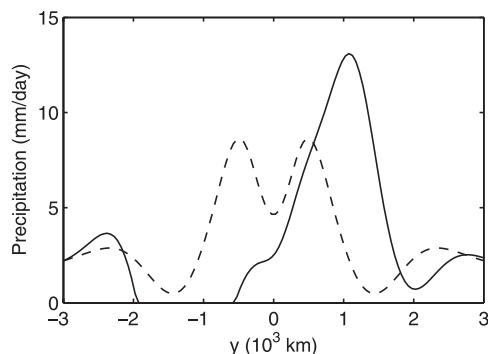

FIG. 11. Precipitation in the symmetric (dashed) and asymmetric (solid) equilibria for a latitudinal distribution with a relative minimum at the equator.

of the wind. The previous sections show the importance of these factors in determining the regime of Hadley circulation and in controlling the position (and number) of ITCZ(s).

In particular, recent experiments using cloud-resolving models have shown that lateral entrainment in clouds is larger than previously expected (Kuang and Bretherton 2006), and its underestimation by current parameterizations of the convection results in a weak sensitivity of the parameterized convection to the free-tropospheric humidity (Derbyshire et al. 2004). In our model, decreasing the sensitivity of convection to free-tropospheric humidity can suppress the asymmetric equilibrium. For example, in the case of a relative SST minimum at the equator, this equilibrium disappears for $\mathcal{E}_q < \lambda'_c \, \mathcal{E}_q^{\text{control}}$ with $\lambda'_c \approx 0.92$, and only the double-ITCZ equilibrium remains. The underestimation of this sensitivity in the GCMs might help explain why symmetric double-ITCZ solutions are sustained during longer periods in the models compared to observations.

4. Summary and discussion

We have used an axisymmetric model of the atmosphere with a truncated vertical structure in an aquaplanet configuration to show that the interaction of dynamics and convection can break the symmetry of the Hadley circulation and account for the existence of an off-equatorial ITCZ, even over an equatorially symmetric SST distribution. Our model exhibits multiple equilibria: one equilibrium with an ITCZ over the equator and two equilibria with an off-equatorial ITCZ; these two asymmetric equilibria are mirror images of each other with respect to the equator. If a relative minimum of SST is added on the equator, the symmetric equilibrium exhibits a double ITCZ while the asymmetric equilibria are almost unchanged.

It appears that dynamical feedbacks are crucial to maintaining an off-equatorial ITCZ in the axisymmetric case. In particular, frictional convergence does provide humidity to the ITCZ. In this respect, the mechanisms at play in our model are somewhat similar to the mechanisms at play in the frictional CISK mechanism. Our model is not a "CISK model" in that the convective closure is based on quasi equilibrium; the closure involves adjustment of the temperature and humidity profiles, rather than explicitly depending on moisture convergence. As a result, the model can behave in ways inconsistent with classical CISK theory. For example, in one of our experiments we shift the off-equatorial ITCZ northward, and the ABL convergence is a negative rather than positive feedback; it drives the return back to equilibrium rather than sustaining the northward shift. An-

other property that one might perhaps associate with CISK is the tendency for a negative gross moist stability so that regions of high moist static energy tend to import moist static energy, sustaining themselves without aid of surface fluxes or radiation. A negative gross moist stability sometimes, although not consistently, occurs in the ITCZ in our results (not shown): generally we have not found the multiple equilibria described here to be easily understood in terms of the moist static energy budget.

We further investigated the processes and feedbacks that explain the existence and stability of these equilibria. It appears that the vertical profile of the wind and that of the diabatic heating are crucial to the existence and stability of the asymmetric equilibria. Furthermore, it appears that the convection has to be quite sensitive to the free-tropospheric ambient moisture to sustain an asymmetric equilibrium. Various studies showed that the ITCZ regime in GCMs is sensitive to the parameterization of convection (Hess et al. 1993) and that the double-ITCZ bias can be mitigated by introduction of a new convective scheme (Zhang and Wang 2006) or by changes in the parameters of a given parameterization (Terray 1998; Bacmeister et al. 2006; Li et al. 2007). Also, the current parameterizations exhibit a weak sensitivity to the free-tropospheric humidity compared to cloud-resolving models (Derbyshire et al. 2004). Improving the parameterizations of convection, particularly in large-scale conditions typical of eastern tropical basins, still seems to hold some promise of cure to the double-ITCZ syndrome.

The multiple equilibria of the full model appear to be directly related to multiple equilibria of atmospheric columns in the dry subtropical regions, as described by a single-column model run using the weak temperature gradient (WTG) approximation at the point of the local tropical precipitation minimum. This indicates that the interaction between convection and large-scale dynamics essential to the existence of the multiple equilibria in the full model can be captured by the local, reduced-dimension approximation embodied by the WTG single-column model. This would seem to make the single-column multiple equilibria (in this model and others) worthy of further study.

The existence of multiple equilibria in our simple model as well as in GCM simulations (Chao and Chen 2004; Barsugli et al. 2005) calls for a systematic investigation of the response of our community's models in aquaplanet configuration to various SST latitudinal distributions. The Aqua-Planet Experiment (APE) (Neale and Hoskins 2000) follows such an approach. Careful analysis of such simulations in a number of models might allow our community to better understand the feedbacks
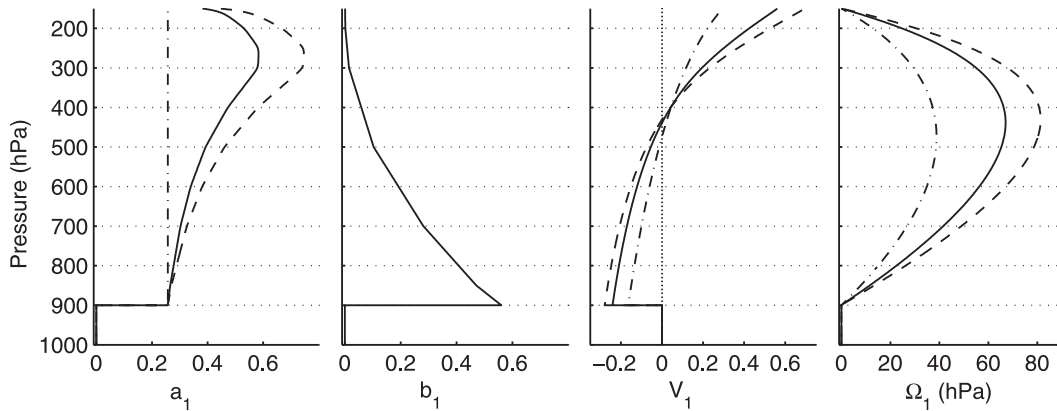
FIG. A1. Free-tropospheric basis functions for temperature a_1 and humidity b_1, horizontal wind V_1, and vertical wind Ω_1 (solid); a_1' and the corresponding momentum functions V_1' and Ω_1' are shown for $l = 0$ (dash–dotted) and for $l = 1.5$ (dashed).

at play in the control of the model tropical convergence zones and suggest solutions to the associated biases in the complete models.

APPENDIX

Model Description

a. Vertical profiles

In the QTCM2, the temperature and humidity are expressed in energy units; that is, temperature in kelvin multiplied by the heat capacity of air at constant pressure C_p and specific humidity (in kg kg^{-1}) multiplied by the latent heat of vaporization L_v. Also, note that the model is presented here in the axisymmetric version used in the present study: the variables do not vary with longitude.

In the free troposphere, the horizontal wind $\mathbf{v} = (u, vv)$, temperature T, and humidity q are expressed as follows:

$$\mathbf{v}(y, p, t) = V_0(p)\mathbf{v}_0(y, t) + V_1(p)\mathbf{v}_1(y, t),$$
$$T(y, p, t) = T_r(p) + a_1(p)T_1(y, t),$$

and

$$q(y, p, t) = q_r(p) + b_1(p)q_1(y, t) \qquad \text{(A1)}$$

for $p_t < p < p_e$, where p_t (p_e) is the pressure at the tropopause (top of the ABL); $T_r(p)$ and $q_r(p)$ are reference profiles [$T_r(p)$ follows a moist adiabat], $b_1(p)$ is the

perturbation structure function for humidity, and the perturbation structure function for temperature $a_1(p)$ is the perturbation of the moist adiabat up to 280 mb, above which cold top effects (Holloway and Neelin 2007) are considered to reduce the perturbation. These free-tropospheric reference profiles are the same as in QTCM1 (Zeng et al. 2000) but modified to begin at the top of the ABL rather than at the nominal surface. The profile for barotropic velocity $V_0(p)$ is constant in pressure: $V_0(p) = 1$. The profile for baroclinic velocity $V_1(p)$ is constructed to be consistent with a_1, assuming that the pressure gradient force obtained from a_1 by hydrostatic balance has the same vertical structure as the other linear terms in the momentum equation. Figure A1 shows the perturbation profiles a_1 and b_1 and the wind profile V_1.

To ensure mass continuity, the vertical velocity can be written

$$\omega(y, p, t) = -\Omega_0(p)\nabla \cdot \mathbf{v}_0(y, t) - \Omega_1(p)\nabla \cdot \mathbf{v}_1(y, t),$$
$$\text{(A2)}$$

where

$$\Omega_i(p) = \int_{p_t}^{p} V_i(\dot{p})\, d\dot{p}, \quad p_t < p < p_e; \qquad \text{(A3)}$$

The V_0 expression gives $\Omega_0(p) = p - p_t$ and, because V_1 represents the baroclinic mode, $\Omega_1(p_e) = 0$: Ω_1 is shown in Fig. A1.

The ABL is considered well mixed. There, $\mathbf{v}$, q, and the dry static energy s are expressed

$$\mathbf{v}(y, p, t) = \mathbf{v}_b(y, t),$$
$$s(y, p, t) = s_{rb} + s_b(y, t),$$

and

$$q(y, p, t) = q_{rb} + q_b(y, t) \qquad (A4)$$

for $p_e < p < p_s$, where p_s is the pressure at the surface; s_{rb} and q_{rb} are reference values for ABL dry static energy and specific humidity. The temperature follows a dry adiabat and can therefore be computed from s.

b. Model equations

The model continuity equation can be reduced to a simple expression: at p_e, we have $\omega(y, p_e, t) = (p_s - p_e)\mathbf{\nabla} \cdot \mathbf{v}_b(y, t) = -(p_e - p_t)\mathbf{\nabla} \cdot \mathbf{v}_0(y, t)$, which yields

$$p_B \mathbf{\nabla} \cdot \mathbf{v}_b(y, t) = -p_F \mathbf{\nabla} \cdot \mathbf{v}_0(y, t), \qquad (A5)$$

where $p_F = p_e - p_t$ is the depth of the free troposphere and $p_B = p_s - p_e$ is the depth of the ABL. Furthermore, since the model is axisymmetric, $\mathbf{\nabla} \cdot \mathbf{v} = \partial_y v$. By integrating from the extremity of the domain (the equatorial β plane's "pole") we can further write

$$\mu v_b(y, t) = -v_0(y, t) \qquad (A6)$$

with $\mu = p_B/p_F$.

For the free troposphere, we assume the vertical structures described above and perform vertical integrations to obtain the model equations, essentially a low-order Galerkin truncation. The model temperature, moisture, and barotropic momentum equations are obtained by vertical averaging of the respective three-dimensional equations over the free troposphere for those variables, while the baroclinic equation is obtained by first multiplying the momentum equation by $V_1(p)$ and then averaging. The equations can be written in either flux or advective form with no significant consequence. As in Sobel and Neelin (2006), we write the equations for the boundary layer variables and the free-tropospheric barotropic velocity in flux form, while we write the equations for free-tropospheric temperature, moisture, and baroclinic velocity in advective form.

The resulting free-tropospheric temperature and moisture equations are

$$\langle a_1 \rangle^F [\partial_t T_1 + \mathbf{v}_0 \cdot \mathbf{\nabla} T_1] + (M_{s0} + s_e - s^\dagger)\mathbf{\nabla} \cdot \mathbf{v}_0$$
$$+ \langle a_1 V_1 \rangle^F \mathbf{v}_1 \cdot \mathbf{\nabla} T_1 + M_{s1}\mathbf{\nabla} \cdot \mathbf{v}_1 = \langle Q_c \rangle^F + \langle Q_R \rangle^F$$
$$+ (s_{rb} + s_b - s_e)\tau_m^{-1} + \langle a_1 \rangle^F k_q \nabla^2 T_1 \qquad (A7)$$

and

$$\langle b_1 \rangle^F [\partial_t q_1 + \mathbf{v}_0 \cdot \mathbf{\nabla} q_1] + (M_{q0} - q_e + q^\dagger)\mathbf{\nabla} \cdot \mathbf{v}_0$$
$$+ \langle b_1 V_1 \rangle^F \mathbf{v}_1 \cdot \mathbf{\nabla} q_1 - M_{q1}\mathbf{\nabla} \cdot \mathbf{v}_1$$
$$= \langle Q_q \rangle^F + (q_{rb} + q_b - q_e)\tau_m^{-1} + \langle b_1 \rangle^F k_q \nabla^2 q_1, \qquad (A8)$$

where $\langle \ \rangle^F$ indicates the free-tropospheric average; subscript e indicates the total value just above ABL top and superscript $\dagger$ the value used to calculate the vertical flux at the boundary layer top; Q_c, Q_q, and Q_R are, respectively, the convective heating, convective moistening, and radiative heating; the term in τ_m^{-1} accounts for mixing at the top of the boundary layer; and k_q is the horizontal diffusivity coefficient for humidity and temperature. We have further defined the gross dry static stabilities and gross moisture stratifications for each mode:

$$M_{si} = M_{\mathrm{sri}} + M_{\mathrm{spi}} T_1$$
$$= -\langle \Omega_i \partial_p s_r \rangle^F - \left\langle \Omega_i \left(\frac{\partial_p a_1 - \kappa a_1}{p} \right) \right\rangle^F T_1,$$
$$M_{qi} = M_{\mathrm{qri}} + M_{\mathrm{qpi}} q_1 = \langle \Omega_i \partial_p q_r \rangle^F + \langle \Omega_i \partial_p b_1 \rangle^F q_1, \quad (A9)$$

where the index i can be either 0 or 1.

The equations for barotropic and baroclinic velocities are

$$\partial_t \mathbf{v}_0 + \mathbf{\nabla} \cdot (\mathbf{v}_0 \mathbf{v}_0) + \langle V_1^2 \rangle^F \mathbf{\nabla} \cdot (\mathbf{v}_1 \mathbf{v}_1) - (\mathbf{\nabla} \cdot \mathbf{v}_0)\mathbf{v}^\dagger$$
$$+ f\mathbf{k} \times \mathbf{v}_0 = -\mathbf{\nabla}(\kappa a_b^{+e} s_b + \kappa \langle a_1^+ \rangle^F T_1 + \phi_s)$$
$$+ (\mathbf{v}_b - \mathbf{v}_e)\tau_m^{-1} + k_v \nabla^2 \mathbf{v}_0 \qquad (A10)$$

and

$$\partial_t \mathbf{v}_1 + \mathbf{v}_0 \cdot \mathbf{\nabla}\mathbf{v}_1 + \mathbf{v}_1 \cdot \mathbf{\nabla}\mathbf{v}_0 + \frac{\langle V_1^3 \rangle^F}{\langle V_1^2 \rangle^F}\mathbf{v}_1 \cdot \mathbf{\nabla}\mathbf{v}_1 + \frac{\langle V_1^3 \rangle^F}{2\langle V_1^2 \rangle^F}(\mathbf{\nabla} \cdot \mathbf{v}_1)\mathbf{v}_1 - \frac{1}{2}\left[\frac{V_{1e}^2}{\langle V_1^2 \rangle^F} - 1 \right](\mathbf{\nabla} \cdot \mathbf{v}_0)\mathbf{v}_1 - \frac{V_{1e}}{\langle V_1^2 \rangle^F}(\mathbf{\nabla} \cdot \mathbf{v}_0)(\mathbf{v}^\dagger - \mathbf{v}_e)$$
$$+ f\mathbf{k} \times \mathbf{v}_1 = -\kappa \mathbf{\nabla} T_1 - \epsilon_1 \mathbf{v}_1 + V_{1e}(\mathbf{v}_b - \mathbf{v}_e)\tau_m^{-1} + k_v \nabla^2 \mathbf{v}_1, \qquad (A11)$$

where $f = \beta y$ is the Coriolis parameter, $\mathbf{k}$ the vertical unit vector, $\kappa = R/C_p$ is the ratio of the gas constant for air R by the heat capacity of air at constant pressure C_p, ϕ_s is the surface geopotential, k_v is the horizontal diffusivity coefficient for momentum, and ϵ_1 is a coefficient that accounts for vertical mixing by small eddies. We

have also introduced the notational shorthand $V_{1e} \equiv V_1(p_e)$. The coefficients a_b^{+e} and a_1^+ come from integrating temperature to obtain the geopotential using hydrostatic balance, and are defined by

$$a_b^{+e} = \int_{P_e}^{p_s} a_b d \ln p = a_b^+(p_e);$$

$$a_1^+(p) = \int_p^{p_e} a_1(p') d \ln p'. \qquad (A12)$$

For the boundary layer, the procedure is essentially the same, but simpler, as each variable has only one mode, and each prognostic variable q, s, $\mathbf{v}$ is assumed uniform on the vertical. We thus have the following equations for ABL dry static energy and specific humidity:

$$\partial_t s_b + \nabla \cdot [\mathbf{v}_b(s_{rb} + s_b)] - s^\dagger \nabla \cdot \mathbf{v}_b = \frac{g}{p_B} H + \langle Q_R \rangle^b$$

$$+ \langle Q_c \rangle^b - \frac{s_{rb} + s_b - s_e}{\mu \tau_m} + k_q \nabla^2 s_b \qquad (A13)$$

and

$$\partial_t q_b + \nabla \cdot [\mathbf{v}_b(q_{rb} + q_b)] - q^\dagger \nabla \cdot \mathbf{v}_b = \frac{g}{p_B} E + \langle Q_q \rangle^b$$

$$- \frac{q_{rb} + q_b - q_e}{\mu \tau_m} + k_q \nabla^2 q_b, \qquad (A14)$$

where E and H are the surface fluxes of latent and sensible heat, respectively, and $\langle \rangle^b$ indicates averaging over the boundary layer.

The ABL velocity obeys

$$\partial_t \mathbf{v}_b + \nabla \cdot (\mathbf{v}_b \mathbf{v}_b) - \mathbf{v}^\dagger \nabla \cdot \mathbf{v}_b + f\mathbf{k} \times \mathbf{v}_b = -\nabla(\kappa \langle a_b^+ \rangle^b s_b$$

$$+ \phi_s) - (\mathbf{v}_b - \mathbf{v}_e)(\mu \tau_m)^{-1} - \epsilon_b \mathbf{v}_b + k_v \nabla^2 \mathbf{v}_b, \qquad (A15)$$

where ϵ_b is a surface drag coefficient. The coefficient of the baroclinic ABL geopotential contribution $\langle a_b^+ \rangle^b$ results from the integration of the hydrostatic equation to obtain the geopotential:

$$\langle a_b^+ \rangle^b = p_B^{-1} \int_{P_e}^{p_s} \int_p^{p_s} a_b d \ln p \, dp. \qquad (A16)$$

Terms involving $s^\dagger$, $q^\dagger$, or $\mathbf{v}^\dagger$ represent vertical advective fluxes at the ABL top. We choose to use an upwind formulation of these terms:

$$X^\dagger = \begin{cases} X_{rb} + X_b & \text{if} \quad \nabla \cdot \mathbf{v}_b < 0 \\ X_e & \text{if} \quad \nabla \cdot \mathbf{v}_b > 0 \end{cases}$$

with $X = s$, q, or $\mathbf{v}$ ($\mathbf{v}_{rb} = 0$).

Using the continuity equation [Eq. (A6)], the surface geopotential gradient $\partial_y \phi_s$ can be diagnosed by adding the meridional components of Eqs. (A10) and (A15) weighted by the depth of the corresponding layer. The resulting expression for the surface geopotential is

$$(1 + \mu)\partial_y \phi_s = -\kappa \partial_y [(\mu \langle a_b^+ \rangle^b + a_b^{+e}) s_b + \langle a_1^+ \rangle^F T_1]$$

$$- f(\mu u_b + u_0) - \epsilon_b \mu v_b - \mu(1 + \mu)\partial_y(v_b^2) - \langle V_1^2 \rangle^F \partial_y(v_1^2). \qquad (A17)$$

In practice, Eq. (A17) is used with Eq. (A15) to compute v_b, and v_0 is diagnosed from v_b using the continuity equation [Eq. (A6)].

c. Model physics

CONVECTION

The convective heating and moistening $\langle Q_c \rangle^F$, $\langle Q_c \rangle^b$, $\langle Q_q \rangle^F$, and $\langle Q_q \rangle^b$ are parameterized using the Betts–Miller scheme (Betts 1986; Betts and Miller 1986) as implemented in the prototype QTCM2 (Sobel and Neelin 2006). In the Betts–Miller scheme, precipitation is proportional to the convective available potential energy $\mathcal{E}$ if the latter is positive, and is zero otherwise. Here $\mathcal{E}$ is the column-integrated difference between a critical temperature profile and the actual temperature profile. When convection occurs, the temperature relaxes toward the critical profile, and humidity relaxes toward an empirically defined critical profile as well. These critical profiles are defined as follows:

$$T^c(p) = T_r^c(p) + A_1(p)(h_b + \delta h_b) \qquad (A18)$$

and

$$q^c(p) = q_r^c(p) + B_1(p)(h_b + \delta h_b), \qquad (A19)$$

where $h_b = s_b + q_b$ and δh_b (<0) is an adjustment variable that allows energy conservation and some downdraft effects. The critical profile of temperature follows a moist adiabat starting at the surface with a moist static energy $h_b + \delta h_b$ inferior to the ambient h_b due to downdraft effects; T_r^c and A_1 are therefore identical to the projection profiles: $T_r^c \equiv T_r$, and $A_1 \equiv a_1$. Here, as in previous studies using the same model (Sobel and Neelin 2006; Bellon and Sobel 2008a,b; Bellon et al. 2008), the critical humidity profiles are taken identical to the basic profiles as well: $q_r^c \equiv q_r$, and $B_1 \equiv b_1$.

This yields the following expression for the convective available potential energy:

$$\mathcal{E} = g^{-1}(p_F \langle A_1 \rangle^F (h_b + \delta h_b) - \langle a_1 \rangle^F T_1 + p_B \sigma \delta h_b), \qquad (A20)$$

where σ is a parameter that partitions δh_b in its temperature component $\sigma \delta h_b$ and its moisture component $(1 - \sigma)\delta h_b$. Here σ therefore also partitions the convective cooling and drying in the boundary layer.

The convective contributions to the energy and water budgets are

$$\langle Q_c \rangle^F = \mathcal{H}(\mathcal{E})\epsilon_c[\langle A_1 \rangle^F (h_b + \delta h_b) - \langle a_1 \rangle^F T_1],$$

$$\langle Q_q \rangle^F = \mathcal{H}(\mathcal{E})\epsilon_c[\langle B_1 \rangle^F (h_b + \delta h_b) - \langle b_1 \rangle^F q_1],$$

$$\langle Q_c \rangle^b = \mathcal{H}(\mathcal{E})\epsilon_c \sigma \delta h_b,$$

and

$$\langle Q_q \rangle^b = \mathcal{H}(\mathcal{E})\epsilon_c (1 - \sigma)\delta h_b, \qquad \text{(A21)}$$

where $\epsilon_c = \tau_c^{-1}$ is a large damping rate for the dissipation of buoyancy by convection and $\mathcal{H}$ is the Heaviside step function [$\mathcal{H}(x) = 0$ if $x < 0$, $\mathcal{H}(x) = 1$ if $x > 0$].

To obtain δh_b, we apply the energy constraint that the net moisture loss must equal the net (dry) enthalpy gain:

$$p_B(\langle Q_c \rangle^b + \langle Q_q \rangle^b) + p_F(\langle Q_c \rangle^F + \langle Q_q \rangle^F) = 0, \qquad \text{(A22)}$$

which yields the following expression for δh_b:

$$\delta h_b = \frac{[-(\langle A_1 \rangle^F + \langle B_1 \rangle^F)h_b + \langle a_1 \rangle^F T_1 + \langle b_1 \rangle^F q_1]}{\mu + \langle A_1 \rangle^F + \langle B_1 \rangle^F}. \qquad \text{(A23)}$$

Condensed water is considered to precipitate immediately, and the precipitation P (in W m^{-2}) is therefore

$$P = -g^{-1}(p_B \langle Q_q \rangle^b + p_F \langle Q_q \rangle^F) = g^{-1}(p_B \langle Q_c \rangle^b$$

$$+ p_F \langle Q_c \rangle^F) = \epsilon_c \mathcal{H}(\mathcal{E})\mathcal{E}. \qquad \text{(A24)}$$

Also, combining Eqs. (A20) and (A23), $\mathcal{E}$ can be written as a linear function of h_b, q_1, and T_1:

$$\mathcal{E} = \mathcal{E}_b h_b + \mathcal{E}_q q_1 + \mathcal{E}_T T_1 \qquad \text{(A25)}$$

with

$$\mathcal{E}_b = \frac{p_B}{g} \frac{\langle A_1 \rangle^F (1 - \sigma) - \langle B_1 \rangle^F \sigma}{\mu + \langle A_1 \rangle^F + \langle B_1 \rangle^F},$$

$$\mathcal{E}_q = \frac{p_F}{g} \langle b_1 \rangle^F \frac{\langle A_1 \rangle^F + \mu\sigma}{\mu + \langle A_1 \rangle^F + \langle B_1 \rangle^F},$$

and

$$\mathcal{E}_T = -\frac{p_F}{g} \langle a_1 \rangle^F \frac{\langle B_1 \rangle^F + \mu(1 - \sigma)}{\mu + \langle A_1 \rangle^F + \langle B_1 \rangle^F}. \qquad \text{(A26)}$$

d. Surface fluxes

Surface fluxes are parameterized by standard bulk formulae:

$$E = \rho_a C_D V_s(q^*(T_s) - q_b) \qquad \text{(A27)}$$

and

$$H = \rho_a C_D V_s(T_s - s_b), \qquad \text{(A28)}$$

where T_s is the SST, $q^*(T_s)$ is the saturation specific humidity at T_s, C_D is the exchange coefficient, ρ_a is the surface air density, and V_s is the surface wind speed. Here V_s is taken to be a function of the boundary layer wind $\mathbf{v}_b$ to include wind-induced mechanisms (Emanuel 1987; Neelin et al. 1987):

$$V_s = \sqrt{G^2 + |\mathbf{v}_b|^2}, \qquad \text{(A29)}$$

where G is the gustiness, a constant wind that accounts for subgrid circulations; it is set to 5 m s^{-1}.

RADIATION

In the free troposphere, we use a Newtonian cooling:

$$\langle Q_R \rangle^F = \frac{T_R - T_1}{\tau_R}, \qquad \text{(A30)}$$

where T_R is a radiative equilibrium temperature (relative to the reference temperature T_r) and τ_R a radiative time scale.

In the boundary layer, we use the scheme

$$\langle Q_R \rangle^b = Q_{Rb0} + \frac{T_s - s_{rb} - s_b}{\tau_{Rb}}, \qquad \text{(A31)}$$

where Q_{Rb0} is a negative constant and τ_{Rb} is the time scale on which the boundary layer is relaxed toward the SST by radiative processes alone, estimated from linearization of a graybody scheme.

e. Simulation design and numerics

The equations are solved using a leapfrog differencing in time with a Robert–Asselin filter, and finite differences in space. The equations for the free-tropospheric baroclinic variables are solved in advective form using first-order upwind differencing, the barotropic and ABL equations in flux form with a centered scheme.

TABLE A1. Model parameter values.

Parameter	Value	Definition
p_s, p_e, p_t	1000, 900, 150 hPa	Pressures at nominal surface, ABL top, and model top (tropopause)
$\langle b_1 \rangle^F, \langle a_1 \rangle^F$	0.178, 0.401	Vertical mean of moisture temperature basis function
b_{1e}, a_{1e}	0.561, 0.257	ABL-top value of moisture and temperature basis function
$V_{1e} \equiv -\langle a_1^+ \rangle^F$	-0.241	
$\langle a_b^+ \rangle^b, a_b^{+e}$	$5.13 \times 10^{-2}, 0.104$	
$\langle V_1^2 \rangle^F, \langle V_1^3 \rangle^F$	$4.71 \times 10^{-2}, 9.66 \times 10^{-3}$	
$\langle b_1 V_1 \rangle^F, \langle a_1 V_1 \rangle^F$	$-2.92 \times 10^{-2}, 2.02 \times 10^{-2}$	
q_{re}, T_{re}	39.0, 298.1 kJ	ABL-top reference moisture and temperature
q_{rb}, s_{rb}	51.6, 303.5 kJ	ABL reference moisture and dry static energy
M_{sr1}, M_{sr0}	2.31, 16.7 kJ	Reference dry static stabilities
M_{sp1}, M_{sp0}	$3.37 \times 10^{-2}, 0.145$	Dry static stability changes per T_1 change
M_{qr1}, M_{qr0}	2.03, 26.6 kJ	Reference gross moisture stratifications
M_{qp1}, M_{qp0}	$2.92 \times 10^{-2}, 0.383$	Gross moisture stratification changes per q_1 change
E_1	1.94×10^{-6} s^{-1}	Frictional damping rate on baroclinic mode
E_b	2.2×10^{-5} s^{-1}	ABL drag coefficient
τ_c, τ_m	0.3 day, 7 days	Convective, ABL-top mixing time scales
σ	0.2	Constant partitioning between convective cooling and drying of ABL
T_R, τ_R	-50 kJ, 25 days	Radiative equilibrium temperature and time scale
Q_{Rb0}, τ_{Rb}	-1.5°K day^{-1}, 5 days	ABL radiative background heating and time scale
ρ_a, C_D	1 kg m^{-3}, 1.5×10^{-3}	Surface air density, exchange coefficient
k_q, k_v	$8 \times 10^5, 2 \times 10^5$ m^2 s^{-1}	Diffusivities for moisture and velocity

The model is integrated over a domain of 20 000 km (10 000 km in each hemisphere), with a time step of 1 min and a spatial resolution of 50 km (400 grid points). As 1° latitude roughly equals 100 km, the latitude will be either given in degrees or kilometers. Increasing the temporal and spatial resolutions does not significantly alter the results. The model is integrated in time until it reaches a steady state (as determined by simple inspection).

Table A1 shows the parameters used in the present study, which are very similar to the parameters used in Sobel and Neelin (2006).

f. WTG model

In the WTG approximation, the temperature is assumed to be fixed by large-scale circulation and gravity waves that reduce the temperature gradients. The tendency and horizontal advection of dry energy are neglected. Here, as a first approximation, we neglect the horizontal advection of humidity because it is a small term in the axisymmetric model in the subtropical region of interest. Neglecting the diffusion tends to push the model in a chaotic regime so the diffusion is replaced by a relaxation toward a reference state with a time scale of $\epsilon^{-1} = 5$ days. Using these simplifications, the free-tropospheric budgets of energy and water can be simplified as follows:

$$(M_{s0} + s_e - s^\dagger) \nabla \cdot \mathbf{v}_0 + M_{s1} \nabla \cdot \mathbf{v}_1$$
$$= \langle Q_c \rangle^F + \langle Q_R \rangle^F + (s_{rb} + s_b - s_e)\tau_m^{-1} - \epsilon T_1 \quad (A32)$$

and

$$\langle b_1 \rangle^F \partial_t q_1 - (M_{q0} - q_e + q^\dagger) \nabla \cdot \mathbf{v}_0 - M_{q1} \nabla \cdot \mathbf{v}_1$$
$$= \langle Q_q \rangle^F + (q_{rb} + q_b - q_e)\tau_m^{-1} - \epsilon q_1. \quad (A33)$$

The ABL budgets can also be simplified:

$$\partial_t s_b + (s_{rb} + s_b - s^\dagger) \nabla \cdot \mathbf{v}_b = \frac{g}{p_B} H + \langle Q_R \rangle^b + \langle Q_c \rangle^b$$
$$- \frac{s_{rb} + s_b - s_e}{\mu \tau_m} - \epsilon s_b \quad (A34)$$

and

$$\partial_t q_b + (q_{rb} + q_b - q^\dagger) \nabla \cdot \mathbf{v}_b = \frac{g}{p_B} E + \langle Q_q \rangle^b$$
$$- \frac{q_{rb} + q_b - q_e}{\mu \tau_m} - \epsilon q_b. \quad (A35)$$

The continuity equation (A6) can be used to relate the barotropic and the ABL divergence:

$$\mu \nabla \mathbf{v}_b = -\nabla \mathbf{v}_0. \quad (A36)$$

REFERENCES

Arakawa, A., and W. H. Schubert, 1974: Interaction of a cumulus cloud ensemble with the large-scale environment, Part I. *J. Atmos. Sci.,* **31,** 674–701.

Bacmeister, J. T., M. J. Suarez, and F. R. Robertson, 2006: Rain reevaporation, boundary layer–convection interactions, and Pacific rainfall patterns in an AGCM. *J. Atmos. Sci.,* **63,** 3383–3403.

Barsugli, J., S. I. Shin, and P. D. Sardeshmukh, 2005: Tropical climate regimes and global climate sensitivity in a simple setting. *J. Atmos. Sci.,* **62,** 1226–1240.

Bellon, G., and A. H. Sobel, 2008a: Instability of the axisymmetric monsoon flow and intraseasonal oscillation. *J. Geophys. Res.,* **113,** D07108, doi:10.1029/2007JD009291.

——, and ——, 2008b: Poleward-propagating intraseasonal monsoon disturbances in an intermediate-complexity axisymmetric model. *J. Atmos. Sci.,* **65,** 470–489.

——, ——, and J. Vialard, 2008: Ocean–atmosphere coupling in the monsoon intraseasonal oscillation: A simple model study. *J. Climate,* **21,** 5254–5270.

Betts, A. K., 1986: A new convective adjustment scheme. Part I: Observational and theoretical basis. *Quart. J. Roy. Meteor. Soc.,* **112,** 677–691.

——, and M. J. Miller, 1986: A new convective adjustment scheme. Part II: Single column tests using GATE wave, BOMEX, ATEX and arctic air-mass data sets. *Quart. J. Roy. Meteor. Soc.,* **112,** 693–709.

Biasutti, M., A. H. Sobel, and Y. Kushnir, 2006: GCM precipitation biases in the tropical Atlantic. *J. Climate,* **19,** 935–958.

Bretherton, C. S., 2007: Challenges in numerical modeling of tropical circulations. *The Global Circulation of the Atmosphere,* T. Schneider and A. H. Sobel, Eds., Princeton University Press, 302–330.

Chao, W. C., and B. Chen, 2004: Single and double ITCZ in an aqua-planet model with constant sea surface temperature and solar angle. *Climate Dyn.,* **22,** 447–459.

Charney, J. G., 1971: Tropical cyclogenesis and the formation of the ITCZ. *Mathematical Problems of Geophysical Fluid Dynamics,* W. H. Reid, Ed., American Mathematical Society, 355–368.

Dai, A. G., 2006: Precipitation characteristics in eighteen coupled climate models. *J. Climate,* **19,** 4605–4630.

Dai, F. S., R. C. Yu, X. H. Zhang, Y. Q. Yu, and J. G. Li, 2003: The impact of low-level cloud over the eastern subtropical Pacific on the "double ITCZ" in LASG FGCM-0. *Adv. Atmos. Sci.,* **20,** 461–474.

Derbyshire, S. H., I. Beau, P. Bechtold, J.-Y. Grandpeix, J.-M. Piriou, J.-L. Redelsperger, and P. M. M. Soares, 2004: Sensitivity of moist convection to environmental humidity. *Quart. J. Roy. Meteor. Soc.,* **130,** 3055–3079.

Emanuel, K. A., 1987: An air–sea interaction model of intraseasonal oscillations in the tropics. *J. Atmos. Sci.,* **44,** 2324–2340.

——, 1991: A scheme for representing cumulus convection in large-scale models. *J. Atmos. Sci.,* **48,** 2313–2329.

——, J. D. Neelin, and C. S. Bretherton, 1994: On large-scale circulations in convecting atmospheres. *Quart. J. Roy. Meteor. Soc.,* **120,** 1111–1143.

Frierson, D. M. W., 2007: The dynamics of idealized convection schemes and their effect on the zonally averaged tropical circulation. *J. Atmos. Sci.,* **64,** 1959–1976.

Goswami, B. N., J. Shukla, E. K. Schneider, and Y. Sud, 1984: Study of the dynamic of the intertropical convergence zone with

a symmetric version of the GLAS climatic model. *J. Atmos. Sci.,* **41,** 5–19.

Gu, G., R. F. Adler, and A. H. Sobel, 2005: The eastern Pacific ITCZ during the boreal spring. *J. Atmos. Sci.,* **62,** 1157–1174.

Hayashi, Y.-Y., and A. Sumi, 1986: The 30–40 day oscillations simulated in an "aqua planet" model. *J. Meteor. Soc. Japan,* **64,** 451–467.

Hess, P. G., D. S. Battisti, and P. J. Rasch, 1993: Maintenance of the intertropical convergence zones and the tropical circulation on a water-covered earth. *J. Atmos. Sci.,* **50,** 691–713.

Holloway, C. R., and J. D. Neelin, 2007: The convective cold top and quasi equilibrium. *J. Atmos. Sci.,* **64,** 1467–1487.

Holton, J. R., J. M. Wallace, and J. A. Young, 1971: On boundary layer dynamics and the ITCZ. *J. Atmos. Sci.,* **28,** 275–280.

Kirtman, B. P., and E. K. Schneider, 2000: A spontaneously generated tropical atmospheric general circulation. *J. Atmos. Sci.,* **57,** 2080–2093.

Kuang, Z., and C. S. Bretherton, 2006: A mass flux scheme view of a high-resolution simulation of a transition from shallow to deep cumulus convection. *J. Atmos. Sci.,* **63,** 1895–1909.

Kuo, H. L., 1974: Further studies of parameterization of influence of cumulus convection on large-scale flow. *J. Atmos. Sci.,* **31,** 1232–1240.

Lau, N.-C., I. M. Held, and J. D. Neelin, 1988: The Madden–Julian oscillation in an idealized general circulation model. *J. Atmos. Sci.,* **45,** 3810–3832.

Li, L. J., B. Wang, Y.-Q. Wang, and H. Wan, 2007: Improvements in climate simulation with modifications to the Tiedtke convective parameterization in the grid-point atmospheric model of IAP LASG (GAMIL). *Adv. Atmos. Sci.,* **24,** 323–335.

Lietzke, C. E., C. Deser, and T. H. Vonder Haar, 2001: Evolutionary structure of the eastern Pacific double ITCZ based on satellite moisture profile retrievals. *J. Climate,* **14,** 743–751.

Lin, J. L., 2007: The double-ITCZ problem in IPCC AR4 coupled GCMs: Ocean–atmosphere feedback analysis. *J. Climate,* **18,** 4497–4525.

Lindzen, R. S., 1974: Wave-CISK in the tropics. *J. Atmos. Sci.,* **31,** 156–179.

——, and S. Nigam, 1987: On the role of the sea surface temperature gradients in forcing the low-level winds and convergence in the tropics. *J. Atmos. Sci.,* **44,** 2418–2436.

Manabe, S., J. Smagorinsky, and R. F. Strickler, 1965: Simulated climatology of a general circulation model with a hydrological cycle. *Mon. Wea. Rev.,* **93,** 769–798.

Mechoso, C. R., and Coauthors, 1995: The seasonal cycle over the tropical Pacific in coupled ocean–atmosphere general circulation models. *Mon. Wea. Rev.,* **123,** 2825–2838.

Moorthi, S., and M. J. Suarez, 1992: Relaxed Arakawa–Schubert: A parameterization of moist convection for general circulation models. *Mon. Wea. Rev.,* **120,** 978–1002.

Neale, R. B., and B. J. Hoskins, 2000: A standard test for AGCMs including their physical parameterizations: I: The proposal. *Atmos. Sci. Lett.,* **1,** 101–107.

Neelin, J. D., and N. Zeng, 2000: A quasi-equilibrium tropical circulation model—Formulation. *J. Atmos. Sci.,* **57,** 1741–1766.

——, I. M. Held, and K. H. Cook, 1987: Evaporation–wind feedback and low-frequency variability in the tropical atmosphere. *J. Atmos. Sci.,* **44,** 2341–2348.

Numaguti, A., 1993: Dynamics and energy balance of the Hadley circulation and the tropical precipitation zones: Significance of the distribution of evaporation. *J. Atmos. Sci.,* **50,** 1874–1887.

Peters, M. E., Z. Kuang, and C. Walker, 2008: Analysis of atmospheric energy transport in ERA-40 and implications for simple models of the mean tropical circulation. *J. Climate,* **21,** 5229–5241.

Pike, A. C., 1971: Intertropical convergence zone studied with an interacting atmosphere and ocean model. *Mon. Wea. Rev.,* **99,** 469–477.

Raymond, D. J., 2000: The Hadley circulation as a radiative-convective instability. *J. Atmos. Sci.,* **57,** 1286–1297.

——, and X. Zeng, 2005: Modelling tropical atmospheric convection in the context of the weak temperature gradient approximation. *Quart. J. Roy. Meteor. Soc.,* **131,** 1301–1320.

——, C. S. Bretherton, and J. Molinari, 2006: Dynamics of the intertropical convergence zone of the east Pacific. *J. Atmos. Sci.,* **63,** 582–597.

Salby, M. L., H. H. Hendon, K. Woodberry, and K. Tanaka, 1991: Analysis of global cloud imagery from multiple satellites. *Bull. Amer. Meteor. Soc.,* **72,** 467–480.

Sessions, S. L., S. Sugaya, D. J. Raymond, and A. H. Sobel, 2010: Multiple equilibria in a cloud resolving model. *J. Geophys. Res.,* in press.

Sikka, D. R., and S. Gadgil, 1980: On the maximum cloud zone and the ITCZ over Indian longitude during southwest monsoon. *Mon. Wea. Rev.,* **108,** 1840–1853.

Sobel, A. H., 2007: Simple models of ensemble-averaged precipitation and surface wind, given the SST. *The Global Circulation of the Atmosphere,* T. Schneider, and A. H. Sobel, Eds., Princeton University Press, 219–251.

——, and C. S. Bretherton, 2000: Modeling tropical precipitation in a single column. *J. Climate,* **13,** 4378–4392.

——, and J. D. Neelin, 2006: The boundary layer contribution to intertropical convergence zones in the quasi-equilibrium tropical circulation model framework. *Theor. Comput. Fluid Dyn.,* **20,** 323–350.

——, and G. Bellon, 2009: The effect of imposed drying on parameterized deep convection. *J. Atmos. Sci.,* **66,** 2085–2096.

——, ——, and J. T. Bacmeister, 2007: Multiple equilibria in a single-column model of the tropical atmosphere. *Geophys. Res. Lett.,* **34,** L22804, doi:10.1029/2007GL031320.

Sumi, A., 1992: Pattern formation of convective activity over the aqua-planet with globally uniform sea surface temperature (SST). *J. Meteor. Soc. Japan,* **70,** 855–876.

Takahashi, K., and D. S. Battisti, 2007: Processes controlling the mean tropical Pacific precipitation pattern. Part I: The Andes and the eastern Pacific ITCZ. *J. Climate,* **20,** 3434–3451.

Terray, L., 1998: Sensitivity of climate drift to atmospheric physical parameterizations in a coupled ocean–atmosphere general circulation model. *J. Climate,* **11,** 1633–1658.

Waliser, D. E., and R. C. J. Somerville, 1994: The preferred latitudes of the intertropical convergence zone. *J. Atmos. Sci.,* **51,** 1619–1639.

Xie, S.-P., 2005: The shape of continents, air–sea interaction, and the rising branch of the Hadley circulation. *The Hadley Circulation: Past, Present and Future,* H. Diaz and R. Bradley, Eds., Cambridge University Press, 489–511.

——, and M. Seki, 1997: Causes of equatorial asymmetry in sea surface temperature over the eastern Pacific. *Geophys. Res. Lett.,* **24,** 2581–2584.

Xu, H. M., Y. Q. Wang, and S. P. Xie, 2004: Effects of the Andes on eastern Pacific climate: A regional atmospheric model study. *J. Climate,* **17,** 589–602.

Zeng, N., J. D. Neelin, and C. Chou, 2000: A quasi-equilibrium tropical circulation model–implementation and simulation. *J. Atmos. Sci.,* **57,** 1767–1796.

Zhang, G. J., and H. J. Wang, 2006: Toward mitigating the double ITCZ problem in NCAR CCSM3. *Geophys. Res. Lett.,* **33,** L06709, doi:10.1029/2005GL025229.

Zhang, X. H., W. Y. Lin, and M. H. Zhang, 2007: Toward understanding the double intertropical convergence zone pathology in coupled ocean–atmosphere general circulation models. *J. Geophys. Res.,* **112,** D12102, doi:10.1029/2006JD007878.